Higher-order effective modeling of periodic heterogeneous beams. II. Derivation of the proper boundary conditions for the interior asymptotic solution

Natacha Buannic, Patrice Cartraud

Higher-order effective modeling of periodic heterogeneous beams. II. Derivation of the proper boundary conditions for the interior asymptotic solution

Natacha Buannic, Patrice Cartraud

Laboratoire Mécanique et Matériaux, Ecole Centrale de Nantes, 1, Rue de la Noë, Nantes, France

This paper constitutes the second part of a study devoted to the 1D modeling of beam-like structures, of arbitrary cross-section with periodic properties along the axis. In the first part, the asymptotic expansion method has been described, and the equations involving the successive terms of the outer solution have been given. In particular, it has been shown that neither the leading term nor the full outer solution are able to satisfy arbitrary prescribed edge data. A specific study is thus necessary and it is presented in this paper.

The method used is the decay analysis initially proposed for homogeneous plates by Gregory and Wan (J. Elast. 14 (1984) 27). This approach consists in deriving the appropriate set of boundary conditions for the outer expansion solution, for any arbitrary edge data (stress, displacement or mixed data). These boundary conditions are obtained from the solution of canonical beam problems, without computing any inner solution. The method is illustrated through numerical examples on a lattice structure. The results obtained prove the importance of a correct treatment of the edge effects, in order that the inclusion of higher-order terms in the beam model serves actually to increase the accuracy of the outer expansion solution.

1. Introduction

The elastostatic behavior of periodic heterogeneous beams has been treated in Part I of this paper. Through the use of the two-scale asymptotic expansion method, the initial 3D problem has been split in a sequence of 3D cellular problems, posed on the period, and 1D macroscopic problems, which provide the effective 1D behavior of the beam. Especially, the way of deriving the higher-order terms of the outer asymptotic expansions is presented, solving successively the 3D and 1D problems. The set of cellular problems is completely defined in Section 4 of Part I, and the equilibrium equations and constitutive relations of the 1D macroscopic problems are given in Section 5. However, the boundary conditions have not

Corresponding author. Tel.: +33-2-4037-2585; fax: +33-2-4037-2573.
E-mail address: patrice.cartraud@ec-nantes.fr (P. Cartraud).

been derived, and it has been only shown that the outer asymptotic expansion cannot satisfy the real prescribed data. Thus, a specific treatment of the boundary conditions is necessary and this is the subject of Part II of this paper.

Several means of deriving the boundary conditions for the interior solution can be found in the literature. A heuristic method consists in satisfying the prescribed data in an approximate manner. Thus, for stress edge data, the boundary conditions can be fulfilled in an integral sense, through the use of Saint-Venant's principle. For displacement edge data, however, this engineering approach relies on choices, such as the definition of the rotation of the cross-section Timoshenko and Goodier (1970). Thus, different interior solutions may be obtained. Furthermore, these approximate boundary conditions can lead to erroneous outer solutions, even far away from the edges Gregory and Wan (1984).

Another approach consists in satisfying exactly the 3D boundary conditions, introducing an *inner* expansion, see e.g. Friedrichs and Dressler (1961), Dauge et al. (1999) for plates, Rigolot (1976) for beams. Nevertheless, this method requires treating boundary layer problems at each order, which is very difficult and tedious. Moreover, in the case where only the overall behavior of the structure is sought, the knowledge of edge effects is not necessary. To this end, the method proposed in Gregory and Wan (1984) enables us to find the *correct* edge data, which ensure the outer expansion to be a good approximate of the 3D solution, far from the edges, without reference to the inner solution. This method, so called the *decay analysis technique*, uses Maxwell–Betti's theorem and provides the set of boundary conditions for the outer expansion, involving the solution of certain canonical problems which can be solved once for all. This method has been initially proposed in the case of a semi-infinite homogeneous isotropic strip Gregory and Wan (1984), and has been extended to the cases of homogeneous beams in Fan and Widera (1992) and of layered orthotropic beams in Duva and Simmonds (1991). We intend here to apply this method to the case of heterogeneous periodic beams.

After a brief review in Section 2 of the main results of the asymptotic expansion method, the decay analysis approach is presented in Section 3. Four kinds of prescribed data are considered herein, and the corresponding boundary conditions for the successive terms of the outer expansion are given. In Section 4, two numerical examples of a truss beam, with respectively a bending/stretching coupling or not, are solved. These applications enable us to illustrate how the outer expansion including end effects through the decay analysis is very close to the exact 3D solution, away from the edges.

2. Governing equations for the interior asymptotic solution

2.1. The 3D heterogeneous problem

We recall that the structure here is a periodic heterogeneous beam, which occupies the domain Ω^ε, see Fig. 1 in Part I. The slenderness axis corresponds to the $\mathbf{e_3}$-direction. The boundary of Ω^ε is defined by $\partial\Omega^\varepsilon = S_0^\varepsilon \cup S_L^\varepsilon \cup \Gamma_b^\varepsilon \cup \Gamma_c^\varepsilon$, with S_0^ε and S_L^ε the two end sections of the beam, while Γ_b^ε and Γ_c^ε are the outer and inner lateral boundary surfaces of the beam.

For later simplification, we assume that the structure is not subjected to any body force and that its lateral boundaries $\Gamma_b^\varepsilon \cup \Gamma_c^\varepsilon$ are traction free. Consequently, the equations of the 3D problem P^ε of linear elasticity are:

$$\begin{cases} \underset{\sim}{\mathbf{div}}_{\mathbf{x}}\, \boldsymbol{\sigma}^\varepsilon = 0 \\ \boldsymbol{\sigma}^\varepsilon = \mathbf{a}^\varepsilon(\underset{\sim}{\mathbf{x}}) : \mathbf{e}^\varepsilon(\underset{\sim}{\mathbf{u}}^\varepsilon) \\ \mathbf{e}^\varepsilon(\underset{\sim}{\mathbf{u}}^\varepsilon) = \mathbf{grad}^{\mathbf{s}}_{\mathbf{x}}(\underset{\sim}{\mathbf{u}}^\varepsilon) \\ \boldsymbol{\sigma}^\varepsilon \cdot \underset{\sim}{\mathbf{n}} = \underset{\sim}{\mathbf{0}} \quad \text{on } \Gamma_b^\varepsilon \cup \Gamma_c^\varepsilon \end{cases} \tag{1}$$

This problem (1) has to be completed with boundary conditions at the end sections S_0^ε and S_L^ε. At S_0^ε, one of the four following sets of prescribed data will be considered:

Case (A) stress data

$$\sigma_{i3}^\varepsilon(x_1,x_2,0)=\bar{\sigma}_{i3}^\varepsilon(x_1,x_2) \tag{2}$$

Case (B) mixed data

$$\begin{cases}\sigma_{\alpha 3}^\varepsilon(x_1,x_2,0)=\bar{\sigma}_{\alpha 3}^\varepsilon(x_1,x_2)\\ u_3^\varepsilon(x_1,x_2,0)=\bar{u}_3^\varepsilon(x_1,x_2)\end{cases} \tag{3}$$

Case (C) mixed data

$$\begin{cases}\sigma_{33}^\varepsilon(x_1,x_2,0)=\bar{\sigma}_{33}^\varepsilon(x_1,x_2)\\ u_\alpha^\varepsilon(x_1,x_2,0)=\bar{u}_\alpha^\varepsilon(x_1,x_2)\end{cases} \tag{4}$$

Case (D) displacement data

$$u_i^\varepsilon(x_1,x_2,0)=\bar{u}_i^\varepsilon(x_1,x_2) \tag{5}$$

and similar conditions will also hold at the other end S_L^ε.

2.2. The interior asymptotic solution

In order to describe the macroscopic solution of the P^ε problem, one can use the asymptotic expansion method with one small parameter for periodic beams, as in Kolpakov (1991). Let us recall here some basic concepts of this method as well as the main results established in Part I of this paper.

Firstly, two scales are involved in the problem: a *microscopic* one which is the scale of the heterogeneities and of the cross-section, and a *macroscopic* scale on which the size of the basic cell is very small. Thus, microscopic variables $y_i=x_i/\varepsilon$ are introduced, as well as a macroscopic one: $z_3=x_3$. Then assumptions on the order of magnitude of the prescribed data are needed. To be more precise, the data in Eqs. (2)–(5) are supposed to satisfy the following relations with respect to ε:

$$\begin{aligned}&\bar{\sigma}_{33}^\varepsilon(x_1,x_2)=\varepsilon^1\cdot\bar{\sigma}_{33}(y_1,y_2) \qquad && \bar{u}_3^\varepsilon(x_1,x_2)=\varepsilon^1\cdot\bar{u}_3(y_1,y_2)\\ &\bar{\sigma}_{\alpha 3}^\varepsilon(x_1,x_2)=\varepsilon^2\cdot\bar{\sigma}_{\alpha 3}(y_1,y_2) && \bar{u}_\alpha^\varepsilon(x_1,x_2)=\bar{u}_\alpha(y_1,y_2)\end{aligned} \tag{6}$$

From the solution of the series of microscopic problems posed on the periodicity cell, it has been established in Part I that the asymptotic expansions of the interior solutions $(\underset{\sim}{\mathbf{u}}^{(I)},\boldsymbol{\sigma}^{(I)})$ can be written formally as:

$$\underset{\sim}{\mathbf{u}}^{(I)}(\underset{\sim}{\mathbf{x}})=\hat{u}_\alpha^0(z_3)\underset{\sim}{\mathbf{e}_\alpha}+\varepsilon^p\left\{\underset{\sim}{\hat{\mathbf{u}}}^p(z_3,\underset{\sim}{\mathbf{y}})+\boldsymbol{\chi}^1(\underset{\sim}{\mathbf{y}})\underset{\sim}{\acute{\mathbf{e}}}^{p-1}(z_3)+\cdots+\boldsymbol{\chi}^{p-1}(\underset{\sim}{\mathbf{y}})\partial_3^{p-2}\underset{\sim}{\acute{\mathbf{e}}}^1(z_3)\right\} \tag{7}$$

$$\boldsymbol{\sigma}^{(I)}(\underset{\sim}{\mathbf{x}})=\varepsilon^p\left\{\boldsymbol{\tau}^1(\underset{\sim}{\mathbf{y}})\underset{\sim}{\acute{\mathbf{e}}}^p(z_3)+\cdots+\boldsymbol{\tau}^p(\underset{\sim}{\mathbf{y}})\partial_3^{p-1}\underset{\sim}{\acute{\mathbf{e}}}^1(z_3)\right\} \tag{8}$$

with $p\geqslant 1$ and where quantities $\underset{\sim}{\acute{\mathbf{e}}}^k$ vanish for $k\leqslant 0$.

Remark 2.1. Relations (7) and (8) are derived from the expressions of $\underset{\sim}{\mathbf{u}}^{\varepsilon}$ and $\boldsymbol{\sigma}^{\varepsilon}$ which have been established in Part I (relations (42) and (43) respectively). However, it must be noticed that, contrary to the latter relations, there is no contribution in Eqs. (7) and (8) of any particular field $\underset{\sim}{\acute{\mathbf{u}}}^{p}{}_{\text{part}}$ or $\acute{\boldsymbol{\tau}}^{p}_{\text{part}}$, since the beam here is free of body force ($\underset{\sim}{\mathbf{f}}^{\varepsilon} = \underset{\sim}{\mathbf{0}}$) and of traction on its lateral boundaries ($\underset{\sim}{\mathbf{g}}^{\varepsilon} = \underset{\sim}{\mathbf{0}}$).

Moreover, the superscript (I) rather than ε is used in Eqs. (7) and (8), in order to distinguish throughout this part of the paper the *interior* solution (I), which satisfy the Eq. (1) but not the boundary conditions, from the exact 3D solution $(\underset{\sim}{\mathbf{u}}^{\varepsilon}, \boldsymbol{\sigma}^{\varepsilon})$, which satisfy (1) as well as the 3D prescribed edge data (i.e. one of the sets (2)–(5) at each end section).

In Eqs. (7) and (8), the displacement fields $\boldsymbol{\chi}^{p}(\underset{\sim}{\mathbf{y}})$ and the stress fields $\boldsymbol{\tau}^{p}(\underset{\sim}{\mathbf{y}})$ constitute the microscopic parts of the outer expansions, and are determined through the solution of the successive cellular problems P^{k}_{cell}, $0 \leqslant k \leqslant p-1$. On the other hand, the fields $\underset{\sim}{\acute{\mathbf{u}}}^{p}(z_3, \underset{\sim}{\mathbf{y}})$ and their respective gradients $\underset{\sim}{\acute{\boldsymbol{\varepsilon}}}^{p}(z_3)$ characterize the macroscopic parts of the outer state $(\underset{\sim}{\mathbf{u}}^{(I)}, \boldsymbol{\sigma}^{(I)})$, and have the following forms ($p \geqslant 1$):

$$\underset{\sim}{\acute{\mathbf{u}}}^{p}(z_3, \underset{\sim}{\mathbf{y}}) = \hat{u}^{p}_{i}(z_3)\underset{\sim}{\mathbf{e_i}} + \varphi^{p}(z_3)[y_1\underset{\sim}{\mathbf{e_2}} - y_2\underset{\sim}{\mathbf{e_1}}] - y_\alpha \partial_3 \hat{u}^{p-1}_{\alpha}(z_3)\underset{\sim}{\mathbf{e_3}} \tag{9}$$

$$\underset{\sim}{\acute{\boldsymbol{\varepsilon}}}^{p}(z_3) = {}^{t}\left\{\partial_3 \hat{u}^{p}_{3}(z_3), \partial_{33}\hat{u}^{p-1}_{1}(z_3), \partial_{33}\hat{u}^{p-1}_{2}(z_3), \partial_3\varphi^{p}(z_3)\right\} \tag{10}$$

The overall response, at each order, is given by the solution of a macroscopic beam problem, involving the macroscopic integrated stress defined by:

$$\underset{\sim}{\acute{\boldsymbol{\sigma}}}^{p}(z_3) = {}^{t}\{N^{p}, M^{p}_{1}, M^{p}_{2}, M^{p}_{3}\} \tag{11}$$

with

$$\begin{aligned} &N^{p}(z_3) = \langle \sigma^{p}_{33} \rangle, \quad M^{p}_{\alpha}(z_3) = \langle -y_\alpha \sigma^{p}_{33} \rangle \\ &M^{p}_{3}(z_3) = \langle -y_2\sigma^{p}_{13} + y_1\sigma^{p}_{23} \rangle \end{aligned} \tag{12}$$

where $\langle \cdot \rangle \equiv (1/l_3)\int_{Y^*} \mathrm{d}Y$ and where l_3 stands for the scaled length of period Y. The equilibrium equations for the pth order homogenized problem, P^{p}_{hom}, are given in Section (5.2) in Part I.

Assuming that the beam is loaded only on its end sections S^{ε}_{0} and S^{ε}_{L}, the latter equilibrium equations can be simplified. It is indeed easy to prove from the first order homogenized problem P^{1}_{hom} that the second gradient of the first order strain vanishes, so that $\partial_{33}\underset{\sim}{\acute{\boldsymbol{\varepsilon}}}^{1}(z_3) = \underset{\sim}{\mathbf{0}}$. Considering now the second order macroscopic problem, the latter result leads to $\partial_{33}\underset{\sim}{\acute{\boldsymbol{\varepsilon}}}^{2}(z_3) = \underset{\sim}{\mathbf{0}}$, so that the equilibrium equations have the same form than at the preceding order. In a recursive manner, for any arbitrary order $p \geqslant 1$, the unknowns $(\hat{u}^{p-1}_{\alpha}, \hat{u}^{p}_{3}, \varphi^{p})$ have to satisfy the four following equations, corresponding respectively to the equilibrium in tension, torsion and bending in the $\underset{\sim}{\mathbf{e_1}}$–$\underset{\sim}{\mathbf{e_3}}$ and $\underset{\sim}{\mathbf{e_2}}$–$\underset{\sim}{\mathbf{e_3}}$ planes, $z_3 \in [0, L]$:

$$\begin{cases} \mathscr{A}^{\text{hom1}}_{11}\partial^{2}_{3}\hat{u}^{p}_{3} + \mathscr{A}^{\text{hom1}}_{12}\partial^{3}_{3}\hat{u}^{p-1}_{1} + \mathscr{A}^{\text{hom1}}_{13}\partial^{3}_{3}\hat{u}^{p-1}_{2} + \mathscr{A}^{\text{hom1}}_{14}\partial^{2}_{3}\varphi^{p} = 0 \\ \mathscr{A}^{\text{hom1}}_{41}\partial^{2}_{3}\hat{u}^{p}_{3} + \mathscr{A}^{\text{hom1}}_{42}\partial^{3}_{3}\hat{u}^{p-1}_{1} + \mathscr{A}^{\text{hom1}}_{43}\partial^{3}_{3}\hat{u}^{p-1}_{2} + \mathscr{A}^{\text{hom1}}_{44}\partial^{2}_{3}\varphi^{p} = 0 \\ \mathscr{A}^{\text{hom1}}_{j1}\partial^{3}_{3}\hat{u}^{p}_{3} + \mathscr{A}^{\text{hom1}}_{j2}\partial^{4}_{3}\hat{u}^{p-1}_{1} + \mathscr{A}^{\text{hom1}}_{j3}\partial^{4}_{3}\hat{u}^{p-1}_{2} + \mathscr{A}^{\text{hom1}}_{j4}\partial^{3}_{3}\varphi^{p} = 0, \quad j = 2, 3 \end{cases} \tag{13}$$

where the 4×4 matrix $\mathscr{A}^{\text{hom1}}$ denotes the first order effective stiffness matrix introduced in Part I.

Therefore, it follows from the addition of the equilibrium Eq. (13) at each order, that the interior asymptotic macroscopic fields $(\hat{u}_{\alpha}(z_3), \hat{u}_3(z_3), \varphi(z_3))$, defined in Eq. (75) in Part I, satisfy the generalized equations of Euler–Bernoulli's theory. It becomes thus obvious that the only difference between the Euler–Bernoulli solution and the interior asymptotic one comes from the expression of the boundary conditions at the ends S^{ε}_{0}, S^{ε}_{L}, as we shall see in the following.

Remark 2.2. A similar result can be found in Gregory and Wan (1984) in the case of homogeneous isotropic infinite plate strip, free of external loads in the interior and free of surface tractions on its upper and lower faces: the interior solution on the mid-plane satisfy the equilibrium equations of Kirchhoff's theory. Moreover, for some prescribed edge data, the authors show that the customarily used Kirchhoff boundary conditions may be recovered, so that, in these cases, the Kirchhoff solution is the exact interior solution on the mid-plane.

In order to complete the macroscopic equilibrium Eq. (13), it remains to derive the boundary conditions. The relations (13) are associated with a coupled stretching-bending-twisting beam model and are composed of two second order differential equations (13) (first and second equations), and two fourth order ones (13) (third and fourth equations). As a consequence, one set of six edge data is expected at each end section S_0^ε, S_L^ε, to ensure the macroscopic problem (13) to be well posed. These boundary conditions have to be expressed as functions of the unknowns of the P^p_{hom} problem, namely $(\hat{u}_\alpha^{p-1}, \hat{u}_3^p, \varphi^p)$ and $\underset{\sim}{\hat{\boldsymbol{\sigma}}}^p(z_3)$ given in Eq. (11).

These edge data can be rigorously derived from the initial prescribed data Eqs. (2)–(5) following the decay analysis method of Gregory and Wan (1984), as it will be seen in Section 3.

3. The decay analysis method

3.1. Principle of the method

The aim of the decay analysis technique proposed in Gregory and Wan (1984) is to derive the correct boundary conditions which have to be prescribed on the interior asymptotic expansions in order that the difference between the latter and the exact 3D solution remains significant only near the edges. For example, when considering the boundary conditions on the end section S_0^ε ($x_3 = 0$), the problem is to find the boundary conditions for the interior solution such that:

$$(\boldsymbol{\sigma}^{(I)}, \underset{\sim}{\mathbf{u}}^{(I)}) - (\boldsymbol{\sigma}^\varepsilon, \underset{\sim}{\mathbf{u}}^\varepsilon) \to 0 \quad \text{as } x_3 \to \infty \tag{14}$$

In Eq. (14), the superscript (I) stands for the *interior* solution while $(\boldsymbol{\sigma}^\varepsilon, \underset{\sim}{\mathbf{u}}^\varepsilon)$ corresponds to the exact 3D elastostatic state which satisfies all the Eq. (1) as well as the prescribed data on the edges.

To obtain the boundary conditions such that the decaying condition (14) holds, the method proposed in Gregory and Wan (1984) relies on the use of the reciprocity theorem (Maxwell–Betti's theorem), as explained below.

The beam with end sections S_0^ε and $S^\varepsilon(x_3)$ is considered, $S^\varepsilon(x_3)$ being the cross-section of abscissa x_3. Let $(\boldsymbol{\sigma}^{(1)}, \underset{\sim}{\mathbf{u}}^{(1)})$ and $(\boldsymbol{\sigma}^{(2)}, \underset{\sim}{\mathbf{u}}^{(2)})$ be two elastostatic states which satisfy the Eq. (1), i.e. the equilibrium equations, compatibility relations as well as the traction free condition of the 3D problem. Applying the reciprocity theorem with these two states leads then to the relation:

$$\int_{S_0^\varepsilon \cup S^\varepsilon(x_3)} \left[\sigma_{ij}^{(1)} u_i^{(2)} - \sigma_{ij}^{(2)} u_i^{(1)}\right] n_j \, \mathrm{d}x_1 \, \mathrm{d}x_2 = 0 \tag{15}$$

The main idea of the method proposed in Gregory and Wan (1984) amounts to choosing for one of the states (1) or (2) the difference between the exact solution of the P^ε problem and the interior solution. For example, let state (1) be that difference, so that:

$$(\boldsymbol{\sigma}^{(1)}, \underset{\sim}{\mathbf{u}}^{(1)}) = (\boldsymbol{\sigma}^{(I)}, \underset{\sim}{\mathbf{u}}^{(I)}) - (\boldsymbol{\sigma}^\varepsilon, \underset{\sim}{\mathbf{u}}^\varepsilon) \tag{16}$$

If we now require the difference $(\boldsymbol{\sigma}^{(1)}, \underset{\sim}{\mathbf{u}}^{(1)})$ to be rapidly decaying when going away from the end section S_0^ε, it follows from Eq. (15) and from the decay condition (14) that:

$$\int_{S_0^\varepsilon} \left[(\sigma_{i3}^{(I)} - \sigma_{i3}^{\varepsilon}) u_i^{(2)} - \sigma_{i3}^{(2)} (u_i^{(I)} - u_i^{\varepsilon}) \right] \mathrm{d}x_1 \, \mathrm{d}x_2 = 0 \tag{17}$$

for all states $(\boldsymbol{\sigma}^{(2)}, \underset{\sim}{\mathbf{u}}^{(2)})$ which satisfy Eq. (1) and which presents a sufficiently *smooth* growth as $x_3 \to \infty$. It is indeed necessary to assume that the state $(\boldsymbol{\sigma}^{(2)}, \underset{\sim}{\mathbf{u}}^{(2)})$ is sufficiently *regular*, in order that the following decay condition holds:

$$\int_{S^\varepsilon(x_3)} \left[\sigma_{ij}^{(1)} u_i^{(2)} - \sigma_{ij}^{(2)} u_i^{(1)} \right] n_j \, \mathrm{d}x_1 \, \mathrm{d}x_2 \to 0 \quad \text{as } x_3 \to \infty \tag{18}$$

In such a way, for any sufficiently regular state $(\boldsymbol{\sigma}^{(2)}, \underset{\sim}{\mathbf{u}}^{(2)})$, the integral on the edge $S^\varepsilon(x_3)$ in Eq. (15) vanishes and relation (17) is obtained.

Remark 3.1. The growth condition on the state (2) is in fact directly connected to the decay form of the state (1), i.e. of the inner solution of the boundary layer problem. In the case of homogeneous isotropic media, this solution is proved to be exponentially decaying. Particularly, for a strip in a plane stress state, it can be expressed with the help of the Papkovich–Fadle eigenfunction fields (Timoshenko and Goodier, 1970; Gregory and Wan, 1984).

This property of exponential decay of the inner part of the solution is also valid in layered media, as shown in Dumontet (1990). In the case of beams, the asymptotic analysis of boundary layer phenomenon is treated in Irago and Viaño (1999) and Irago (1999). A general review of the developments concerning end effects and estimates for their decay rate in isotropic, anisotropic and composite structural elements can be found in Horgan (1989, 1996), and references herein.

Lastly, the case of heterogeneous periodic lattice structures is treated in Stephen and Wang (1996), where a method to evaluate the decay rate is proposed. However, this difficult subject of the decay rate of the state (1) will not be considered in this paper. Therefore, it will only be assumed that this state (1) decays sufficiently rapidly in order to ensure the validity of relation (17), i.e. the vanishing in Eq. (15) of the integral on $S^\varepsilon(x_3)$ when treating the opposite end S_0^ε. For a beam of finite length, the decay condition (14) is practically satisfied provided that the length of the beam is sufficiently large in comparison with the size of the end effects. Thus, there is an interior zone in the beam where edge effects coming from each end section vanish.

Since Eq. (17) has to be satisfied for any regular state $(\boldsymbol{\sigma}^{(2)}, \underset{\sim}{\mathbf{u}}^{(2)})$, it follows that the relation (17) will provide the necessary conditions on the interior fields $(\boldsymbol{\sigma}^{(I)}, \underset{\sim}{\mathbf{u}}^{(I)})$ so that the edge effects decay rapidly, as we shall see in Section 3.2.

3.2. The proper boundary conditions for the interior solution

Let us now exploit the Eq. (17) to derive the six expected boundary conditions for the outer expansions $(\boldsymbol{\sigma}^{(I)}, \underset{\sim}{\mathbf{u}}^{(I)})$. In a second step, in Section 3.3, the boundary conditions at each order will be given. Besides these outer solutions, the exact fields $(\boldsymbol{\sigma}^{\varepsilon}, \underset{\sim}{\mathbf{u}}^{\varepsilon})$ and the regular fields $(\boldsymbol{\sigma}^{(2)}, \underset{\sim}{\mathbf{u}}^{(2)})$ are involved in Eq. (17). The exact fields satisfy the prescribed data on S_0^ε, while state (2) is a priori any regular state, as mentioned above, see also Remark 3.1. The problem of the choice of such states (2) will now be considered.

Firstly, it must be noticed that for a given set of prescribed data Eqs. (2)–(5), some components of $\sigma_{i3}^{\varepsilon}$ or u_i^{ε} in Eq. (17) are unknown (e.g. u_i^{ε} in Case (A)). As a consequence, the state (2) has to be selected in such a way that the corresponding components $u_i^{(2)}$ or $\sigma_{i3}^{(2)}$ vanish (e.g. $\sigma_{i3}^{(2)} = 0$ in Case (A)). Therefore, the state (2) is a regular state satisfying the 3D homogeneous prescribed data at S_0^ε (e.g. since $\sigma_{i3}^{\varepsilon} = \bar{\sigma}_{i3}^{\varepsilon}$ in Case (A) then $\sigma_{i3}^{(2)} = 0$).

These homogeneous boundary conditions can be obtained when considering n rigid body displacements ($0 \leqslant n \leqslant 6$), thus providing n states (2) such that $\boldsymbol{\sigma}^{(2)} = 0$ and $\underset{\sim}{\mathbf{u}}^{(2)}$ equal to a rigid displacement.

As explained at the end of Section 2, six boundary conditions are needed at each end section in order that each macroscopic problem (13) is well posed, so that $(6-n)$ other boundary conditions have to be derived. The latter may be obtained considering the states (2) among the solutions of a semi-infinite beam with the homogeneous boundary conditions at one end, and under a unit tension, a bending moment (in $\underset{\sim}{\mathbf{e_1}}$–$\underset{\sim}{\mathbf{e_3}}$ and $\underset{\sim}{\mathbf{e_2}}$–$\underset{\sim}{\mathbf{e_3}}$ planes), a flexure (with transverse shearing force in $\underset{\sim}{\mathbf{e_1}}$–$\underset{\sim}{\mathbf{e_3}}$ and $\underset{\sim}{\mathbf{e_2}}$–$\underset{\sim}{\mathbf{e_3}}$ planes) and a torque at infinity. The above-described procedure will now be applied successively to the sets of prescribed data (A)–(D), respectively given in Eqs. (2)–(5).

Case (A): In this case, the homogeneous boundary conditions are $\sigma_{3i}^{(2)}(x_1, x_2, 0) = 0$ so that the states (2) are given by the six rigid body displacements. Inserting these states in Eq. (17) and taking into account the assumptions (6), one obtains:

$$\begin{cases} \int_{S_0} \sigma_{33}^{(I)} \, \mathrm{d}y_1 \, \mathrm{d}y_2 = \varepsilon \int_{S_0} \bar{\sigma}_{33} \, \mathrm{d}y_1 \, \mathrm{d}y_2 \\ \int_{S_0} \sigma_{\alpha 3}^{(I)} \, \mathrm{d}y_1 \, \mathrm{d}y_2 = \varepsilon^2 \int_{S_0} \bar{\sigma}_{\alpha 3} \, \mathrm{d}y_1 \, \mathrm{d}y_2 \\ \int_{S_0} y_\alpha \sigma_{33}^{(I)} \, \mathrm{d}y_1 \, \mathrm{d}y_2 = \varepsilon \int_{S_0} y_\alpha \bar{\sigma}_{33} \, \mathrm{d}y_1 \, \mathrm{d}y_2 \\ \int_{S_0} (y_1 \sigma_{23}^{(I)} - y_2 \sigma_{13}^{(I)}) \, \mathrm{d}y_1 \, \mathrm{d}y_2 = \varepsilon^2 \int_{S_0} (y_1 \bar{\sigma}_{23} - y_2 \bar{\sigma}_{13}) \, \mathrm{d}y_1 \, \mathrm{d}y_2 \end{cases} \tag{19}$$

So in that case, Saint-Venant's principle is justified, since the boundary conditions involve load resultants.

The expression (19) involves the resultant forces and resultant moments of the outer stress $\boldsymbol{\sigma}^{(I)}$ on the scaled section S_0. Nevertheless, the macroscopic beam stresses appearing in the successive macroscopic problems, i.e. the stresses contained in $\underset{\sim}{\acute{\boldsymbol{\sigma}}}^k$ as well as the shear forces $T_\alpha^k = \langle \sigma_{\alpha 3}^k \rangle$, are obtained following an average process over the scaled period $\underset{\sim}{Y}$, see Eq. (12). It is thus necessary to connect the average over the period with the integral over the lateral section ∂Y_a of the period, in order to express Eq. (19) as a function of the macroscopic beam stresses.

These relationships are established in Buannic (2000), where it is proved that each component of the macroscopic stresses $\{N^k, \underset{\sim}{\mathbf{M}}^k, T_\alpha^{k+1}\}$ is in fact equal to the value of the corresponding integrated stress on the left side $\partial Y_a(-l_3/2)$ of the period. Thus, if the heterogeneous structure presents a whole number of periods, relation (19) can be written as:

$$\begin{cases} N^{(I)}(0) = \varepsilon \int_{S_0} \bar{\sigma}_{33} \, \mathrm{d}y_1 \, \mathrm{d}y_2 \\ T_\alpha^{(I)}(0) = \varepsilon^2 \int_{S_0} \bar{\sigma}_{\alpha 3} \, \mathrm{d}y_1 \, \mathrm{d}y_2 \\ M_\alpha^{(I)}(0) = \varepsilon \int_{S_0} -y_\alpha \bar{\sigma}_{33} \, \mathrm{d}y_1 \, \mathrm{d}y_2 \\ M_3^{(I)}(0) = \varepsilon^2 \int_{S_0} (y_1 \bar{\sigma}_{23} - y_2 \bar{\sigma}_{13}) \, \mathrm{d}y_1 \, \mathrm{d}y_2 \end{cases} \tag{20}$$

Case (B): For this case, the states (2) have to satisfy $\sigma_{\alpha 3}^{(2)}(x_1, x_2, 0) = u_3^{(2)}(x_1, x_2, 0) = 0$. Consequently, one can select as state (2) the three rigid body displacements corresponding to the two translations in the $\underset{\sim}{\mathbf{e}_\alpha}$-directions and the rotation about the $\underset{\sim}{\mathbf{e_3}}$-axis, which yields:

$$\begin{cases} T_\alpha^{(I)}(0) = \varepsilon^2 \int_{S_0} \bar{\sigma}_{\alpha 3} \, \mathrm{d}y_1 \, \mathrm{d}y_2, \\ M_3^{(I)}(0) = \varepsilon^2 \int_{S_0} (y_1 \bar{\sigma}_{23} - y_2 \bar{\sigma}_{13}) \, \mathrm{d}y_1 \, \mathrm{d}y_2 \end{cases} \tag{21}$$

The three other states (2) correspond respectively to the Saint-Venant unit tension and bending solutions, denoted with the superscript (VE) and (VB_α). So Eq. (17) provides:

$$\int_{S_0} \left[(\sigma_{\alpha 3}^{(I)} - \varepsilon^2 \bar{\sigma}_{\alpha 3}) u_\alpha^{(2)} - \sigma_{33}^{(2)} (u_3^{(I)} - \varepsilon \bar{u}_3) \right] \mathrm{d}y_1 \, \mathrm{d}y_2 = 0 \quad \text{with } .^{(2)} \equiv .^{(\mathrm{VE})}, .^{(\mathrm{VB}_\alpha)} \tag{22}$$

Case (C): Considering here the three rigid body displacements (translation $\underset{\sim}{\mathbf{e}_3}$ and rotations about $\underset{\sim}{\mathbf{e}_\alpha}$), we obtain:

$$\begin{cases} N^{(I)}(0) = \varepsilon \int_{S_0} \bar{\sigma}_{33}\, \mathrm{d}y_1\, \mathrm{d}y_2 \\ M_\alpha^{(I)}(0) = \varepsilon \int_{S_0} -y_\alpha \bar{\sigma}_{33}\, \mathrm{d}y_1\, \mathrm{d}y_2 \end{cases} \tag{23}$$

Then the state (2) is taken to be successively the Saint-Venant unit torsion and flexures solutions, denoted with the superscripts (VT) and (VF_α) respectively. Eq. (17) then yields:

$$\int_{S_0} \left[(\sigma_{33}^{(I)} - \varepsilon \bar{\sigma}_{33}) u_3^{(2)} - \sigma_{\alpha 3}^{(2)} (u_\alpha^{(I)} - \bar{u}_\alpha) \right] \mathrm{d}y_1\, \mathrm{d}y_2 = 0 \quad \text{with} \quad .^{(2)} \equiv .^{(\mathrm{VT})}, .^{(\mathrm{VF}_\alpha)} \tag{24}$$

Case (D): In this case, the homogeneous boundary conditions correspond to a built-in (cantilevered) at the end S_0, which prevents us from selecting any rigid body displacement as state (2). Consequently, the states (2) are the six fundamental solutions of the cantilevered beam, in a state of unit tension (BE), bending (BB_α), flexure (BF_α) and torsion (BT). So, from Eq. (17), the following boundary conditions are derived for the outer expansion:

$$\int_{S_0} \sigma_{i3}^{(2)} (u_i^{(I)} - \bar{u}_i^{e}) \, \mathrm{d}y_1\, \mathrm{d}y_2 = 0 \quad \text{with} \quad .^{(2)} \equiv .^{(\mathrm{BE})}, .^{(\mathrm{BB}_\alpha)}, .^{(\mathrm{BF}_\alpha)}, .^{(\mathrm{BT})} \tag{25}$$

3.3. Derivation of the boundary conditions for the successive terms of the outer expansions

Let us see in detail how to proceed to obtain the boundary conditions for each term of the outer expansion.

Case (A) From Eq. (20), one has directly:

$$\begin{cases} N^1(0) = \int_{S_0} \bar{\sigma}_{33}\, \mathrm{d}y_1\, \mathrm{d}y_2 \\ T_\alpha^2(0) = \int_{S_0} \bar{\sigma}_{\alpha 3}\, \mathrm{d}y_1\, \mathrm{d}y_2 \\ M_\alpha^1(0) = \int_{S_0} -y_\alpha \bar{\sigma}_{33}\, \mathrm{d}y_1\, \mathrm{d}y_2 \\ M_3^1(0) = 0 \end{cases} \tag{26}$$

which are the boundary conditions for the P_{hom}^1 problem.

In the same manner, one obtains from Eq. (20) that the boundary conditions for the P_{hom}^2 problem are:

$$\begin{cases} N^2(0) = T_\alpha^3(0) = M_\alpha^2(0) = 0 \\ M_3^2(0) = \int_{S_0} (y_1 \bar{\sigma}_{23} - y_2 \bar{\sigma}_{13})\, \mathrm{d}y_1\, \mathrm{d}y_2 \end{cases} \tag{27}$$

and for the P_{hom}^k problem, $k \geqslant 3$, one finds homogeneous boundary conditions, i.e.:

$$N^k(0) = T_\alpha^{k+1}(0) = M_i^k(0) = 0 \tag{28}$$

As a consequence, relations (26)–(28) give a rigorous justification for invoking the Saint-Venant principle to ensure the rapid decay of the inner solution.

In the Cases B–D, the integrals (22), (24) and (25) have to be computed. On one hand, one inserts in the latter integrals the outer expansions for $(\underset{\sim}{\mathbf{u}}^{(I)}, \boldsymbol{\sigma}^{(I)})$, given in Eqs. (7) and (8) respectively. On the other hand, the end values of the states (2) have to be determined. The Saint-Venant solutions, involved in Cases B and C, may have an analytical form, but only for homogeneous isotropic beams, and can be checked out from any standard elasticity book, see also Fan (1989). In Gregory and Gladwell (1982), a method is proposed in order to determine in the case of plane strain problems the stresses and stress intensity factors at the fixed end of a cantilever beam under tension, bending or flexure at infinity. In particular, the method given there

enables us to take into account the stress singularities at the corners of the fixed end. For the heterogeneous beams under consideration here, the end values of the states (2) are computed from a 3D finite element model of the beam constituted with a sufficiently large number of periods.

Besides, from the overall equilibrium of the beam, considering either the fundamental Saint-Venant solutions or the cantilever beam ones, the following relations hold:

$$\begin{aligned}
&\int_{S_0} \sigma_{i3}^{(\mathrm{jE})}\,\mathrm{d}y_1\,\mathrm{d}y_2 = \delta_{i3}, \qquad \int_{S_0} y_\alpha \underset{\sim}{\mathbf{e}_\alpha} \wedge \sigma_{i3}^{(\mathrm{jE})} \underset{\sim}{\mathbf{e}_i}\,\mathrm{d}y_1\,\mathrm{d}y_2 = 0\\
&\int_{S_0} \sigma_{i3}^{(\mathrm{jB}_\alpha)}\,\mathrm{d}y_1\,\mathrm{d}y_2 = 0, \qquad \int_{S_0} -y_\beta \sigma_{33}^{(\mathrm{jB}_\alpha)}\,\mathrm{d}y_1\,\mathrm{d}y_2 = \delta_{\alpha\beta}\\
&\int_{S_0} \left(y_1 \sigma_{23}^{(\mathrm{jB}_\alpha)} - y_2 \sigma_{13}^{(\mathrm{jB}_\alpha)}\right)\mathrm{d}y_1\,\mathrm{d}y_2 = 0\\
&\int_{S_0} \sigma_{i3}^{(\mathrm{jF}_\alpha)}\,\mathrm{d}y_1\,\mathrm{d}y_2 = \delta_{i\alpha}, \qquad \int_{S_0} y_\beta \underset{\sim}{\mathbf{e}_\beta} \wedge \sigma_{i3}^{(\mathrm{jF}_\alpha)} \underset{\sim}{\mathbf{e}_i}\,\mathrm{d}y_1\,\mathrm{d}y_2 = 0\\
&\int_{S_0} \sigma_{i3}^{(\mathrm{jT})}\,\mathrm{d}y_1\,\mathrm{d}y_2 = 0, \qquad \int_{S_0} y_\alpha \underset{\sim}{\mathbf{e}_\alpha} \wedge \sigma_{i3}^{(\mathrm{jT})} \underset{\sim}{\mathbf{e}_i}\,\mathrm{d}y_1\,\mathrm{d}y_2 = \delta_{i3} \underset{\sim}{\mathbf{e}_i}
\end{aligned} \tag{29}$$

with (j.) = (V.), (B.), and δ the Kronecker symbol. Let us consider successively the Cases B–D.

Case (B): First, let us derive the boundary conditions for the macroscopic shear forces and torque. Recalling that the first order shearing forces $T_\alpha^1(z_3)$ are found to be zero (see Remark 5.2 in Part I), it follows from Eq. (21):

$$\begin{aligned}
&T_\alpha^2(0) = \int_{S_0} \bar{\sigma}_{\alpha 3}\,\mathrm{d}y_1\,\mathrm{d}y_2, \qquad M_3^1(0) = 0\\
&T_\alpha^3(0) = 0, \qquad M_3^2(0) = \int_{S_0} (y_1 \bar{\sigma}_{23} - y_2 \bar{\sigma}_{13})\,\mathrm{d}y_1\,\mathrm{d}y_2\\
&T_\alpha^{k+1}(0) = M_3^k(0) = 0 \quad \text{for } k \geqslant 3
\end{aligned} \tag{30}$$

It remains to express the boundary conditions for the macroscopic outer displacement $u^{(I)}$. Replacing in Eq. (22) the quantities $\sigma_{\alpha 3}^{(I)}$ and $u_3^{(I)}$ by their respective formal expansion (8) and (7), yields:

$$\int_{S_0} \left[(\varepsilon \sigma_{\alpha 3}^1 + \varepsilon^2 \sigma_{\alpha 3}^2 + \cdots - \varepsilon^2 \bar{\sigma}_{\alpha 3}) u_\alpha^{(2)} - \sigma_{33}^{(2)} (\varepsilon u_3^1 + \varepsilon^2 u_3^2 + \cdots - \varepsilon \bar{u}_3)\right] \mathrm{d}y_1\,\mathrm{d}y_2 = 0 \quad \text{with } .^{(2)} \equiv .^{(\mathrm{VE})}, .^{(\mathrm{VB}_\alpha)} \tag{31}$$

Then, equating to zero the coefficients of the same power of ε, one obtains the boundary conditions corresponding to the successive terms of the outer expansions of $u^{(I)}$.

First order boundary conditions: Firstly, we consider the relation (31) at the first power of ε. The leading terms of the outer expansions are found to be:

$$u_3^1(z_3, \underset{\sim}{\mathbf{y}}) = \hat{u}_3^1(z_3) - y_\alpha \partial_3 \hat{u}_\alpha^0(z_3) \tag{32}$$

$$\sigma_{ij}^1(z_3, \underset{\sim}{\mathbf{y}}) = \tau_{ij\mathbf{m}}^1(\underset{\sim}{\mathbf{y}}).\dot{e}_{\mathbf{m}}^1(z_3) \quad \text{with } 1 \leqslant \mathbf{m} \leqslant 4 \tag{33}$$

Therefore, considering successively the Saint-Venant solutions for the extension (VE) and the bending (VB$_\beta$) as state (2) in Eq. (31), and using the properties (29), it follows that:

$$\hat{u}_3^1(0) - \left(\int_{S_0} \tau_{\alpha 3\mathbf{m}}^1 u_\alpha^{(\mathrm{VE})}\,\mathrm{d}y_1\,\mathrm{d}y_2\right) \cdot \dot{e}_{\mathbf{m}}^1(0) = \int_{S_0} \bar{u}_3 \sigma_{33}^{(\mathrm{VE})}\,\mathrm{d}y_1\,\mathrm{d}y_2 \tag{34}$$

$$\partial_3 \hat{u}_\beta^0(0) - \left(\int_{S_0} \tau_{\alpha 3 \mathbf{m}}^1 u_\alpha^{(\mathrm{VB}_\beta)} \, \mathrm{d}y_1 \, \mathrm{d}y_2 \right) \cdot \acute{e}_{\mathbf{m}}^1(0) = \int_{S_0} \bar{u}_3 \sigma_{33}^{(\mathrm{VB}_\beta)} \, \mathrm{d}y_1 \, \mathrm{d}y_2 \tag{35}$$

It can be noticed that the boundary conditions (34) do not constitute conventional edge data since they involve the end values of the macroscopic beam strain $\underset{\sim}{\acute{\mathbf{e}}}^1(0)$ besides the macroscopic axial displacement $\hat{u}_3^1(0)$ and the two macroscopic rotations $\partial_3 \hat{u}_\beta^0(0)$. As a consequence, relations (34) correspond to *coupled* boundary conditions between $\hat{u}_3^1(0)$, $\partial_3 \hat{u}_\beta^0(0)$, the extension $\partial_3 \hat{u}_3^1(0)$, the two curvatures $\partial_{33} \hat{u}_\beta^0(0)$ and the twisting rate $\partial_3 \varphi^1(0)$.

Remark 3.2. In the homogeneous isotropic case, the integrals in the left hand sides of Eq. (34) are different from 0 only for $\mathbf{m} = 4$. Moreover, in that particular case and under assumption (6), it appears that $\acute{e}_4^1(z_3) = \partial_3 \varphi^1(z_3) = 0$, see Part I (Remark 5.3 and Section 5.1.4). As a consequence, classical boundary conditions are recovered. Similar results are obtained in the case of homogeneous isotropic plate in plane strain analysis in Gregory and Wan (1984).

Second order boundary conditions: At the next order, the outer solutions are:

$$u_3^2(z_3, \underset{\sim}{\mathbf{y}}) = \hat{u}_3^2(z_3) - y_\alpha \partial_3 \hat{u}_\alpha^1(z_3) + \chi_{3\mathbf{m}}^1(\underset{\sim}{\mathbf{y}}) \cdot \acute{e}_{\mathbf{m}}^1(z_3) \tag{36}$$

$$\sigma_{ij}^2(z_3, \underset{\sim}{\mathbf{y}}) = \tau_{ij\mathbf{m}}^1(\underset{\sim}{\mathbf{y}}) \cdot \acute{e}_{\mathbf{m}}^2(z_3) + \tau_{ij\mathbf{m}}^2(\underset{\sim}{\mathbf{y}}) \cdot \partial_3 \acute{e}_{\mathbf{m}}^1(z_3) \tag{37}$$

Consequently, in the same manner as for the first order, the boundary conditions for the second order macroscopic problem are found to be:

$$\hat{u}_3^2(0) - \left(\int_{S_0} \tau_{\alpha 3 \mathbf{m}}^1 u_\alpha^{(\mathrm{VE})} \, \mathrm{d}y_1 \, \mathrm{d}y_2 \right) \cdot \acute{e}_{\mathbf{m}}^2(0) = \int_{S_0} \left[(\tau_{\alpha 3 \mathbf{m}}^2 \cdot \partial_3 \acute{e}_{\mathbf{m}}^1(0) - \bar{\sigma}_{\alpha 3}) u_\alpha^{(\mathrm{VE})} - \chi_{3\mathbf{m}}^1 \cdot \acute{e}_{\mathbf{m}}^1(0) \sigma_{33}^{(\mathrm{VE})} \right] \mathrm{d}y_1 \, \mathrm{d}y_2 \tag{38}$$

$$\partial_3 \hat{u}_\beta^1(0) - \left(\int_{S_0} \tau_{\alpha 3 \mathbf{m}}^1 u_\alpha^{(\mathrm{VB}_\beta)} \, \mathrm{d}y_1 \, \mathrm{d}y_2 \right) \cdot \acute{e}_{\mathbf{m}}^2(0) = \int_{S_0} \left[(\tau_{\alpha 3 \mathbf{m}}^2 \cdot \partial_3 \acute{e}_{\mathbf{m}}^1(0) - \bar{\sigma}_{\alpha 3}) u_\alpha^{(\mathrm{VB}_\beta)} - \chi_{3\mathbf{m}}^1 \cdot \acute{e}_{\mathbf{m}}^1(0) \sigma_{33}^{(\mathrm{VB}_\beta)} \right] \mathrm{d}y_1 \, \mathrm{d}y_2 \tag{39}$$

kth order boundary conditions, $k \geqslant 3$

In a recursive manner, since $\partial_{33} \underset{\sim}{\acute{\mathbf{e}}}^p = \underset{\sim}{\mathbf{0}}$ for any $p \geqslant 1$ (see Section 2.2), one has:

$$u_3^k(z_3, \underset{\sim}{\mathbf{y}}) = \hat{u}_3^k(z_3) - y_\alpha \partial_3 \hat{u}_\alpha^{k-1}(z_3) + \chi_{3\mathbf{m}}^1(\underset{\sim}{\mathbf{y}}) \cdot \acute{e}_{\mathbf{m}}^{k-1}(z_3) + \chi_{3\mathbf{m}}^2(\underset{\sim}{\mathbf{y}}) \cdot \partial_3 \acute{e}_{\mathbf{m}}^{k-2}(z_3) \tag{40}$$

$$\sigma_{ij}^k(z_3, \underset{\sim}{\mathbf{y}}) = \tau_{ij\mathbf{m}}^1(\underset{\sim}{\mathbf{y}}) \cdot \acute{e}_{\mathbf{m}}^k(z_3) + \tau_{ij\mathbf{m}}^2(\underset{\sim}{\mathbf{y}}) \cdot \partial_3 \acute{e}_{\mathbf{m}}^{k-1}(z_3) \tag{41}$$

The following conditions are thus derived:

$$\hat{u}_3^k(0) - \left(\int_{S_0} \tau_{\alpha 3 \mathbf{m}}^1 u_\alpha^{(\mathrm{VE})} \, \mathrm{d}y_1 \, \mathrm{d}y_2 \right) \cdot \acute{e}_{\mathbf{m}}^k(0) = \int_{S_0} \Big[(\tau_{\alpha 3 \mathbf{m}}^2 \cdot \partial_3 \acute{e}_{\mathbf{m}}^{k-1}(0)) u_\alpha^{(\mathrm{VE})} - (\chi_{3\mathbf{m}}^1 \cdot \acute{e}_{\mathbf{m}}^{k-1}(0) + \chi_{3\mathbf{m}}^2 \cdot \partial_3 \acute{e}_{\mathbf{m}}^{k-2}(0)) \sigma_{33}^{(\mathrm{VE})} \Big] \mathrm{d}y_1 \, \mathrm{d}y_2 \tag{42}$$

$$\partial_3\hat{u}_\beta^{k-1}(0) - \left(\int_{S_0} \tau^1_{\alpha 3\mathbf{m}} u_\alpha^{(\mathrm{VB}_\beta)}\,\mathrm{d}y_1\,\mathrm{d}y_2\right)\cdot \acute{e}^k_{\mathbf{m}}(0) = \int_{S_0}\Big[(\tau^2_{\alpha 3\mathbf{m}}\cdot\partial_3\acute{e}^{k-1}_{\mathbf{m}}(0))u_\alpha^{(\mathrm{VB}_\beta)} - (\chi^1_{3\mathbf{m}}\cdot\acute{e}^{k-1}_{\mathbf{m}}(0) + \chi^2_{3\mathbf{m}}\cdot\partial_3\acute{e}^{k-2}_{\mathbf{m}}(0))\sigma_{33}^{(\mathrm{VB}_\beta)}\Big]\,\mathrm{d}y_1\,\mathrm{d}y_2 \tag{43}$$

We recall that the unknowns of the P^k_{hom} problem are $\{\hat{u}_3^k, \hat{u}_\alpha^{k-1}, \varphi^k\}$, as well as $\{\underset{\sim}{\acute{\mathbf{e}}}^k\} =^t \{\partial_3\hat{u}_3^k, \partial_{33}\hat{u}_\alpha^{k-1}, \partial_3\varphi^k\}$ and $\{\underset{\sim}{\acute{\boldsymbol{\sigma}}}^k\} =^t \{N^k, T_\alpha^{k+1}, \underset{\sim}{\mathbf{M}}^k\}$.

Furthermore, when this problem is under consideration, the preceding problems P^j_{hom}, for $1 \leqslant j \leqslant k-1$, as well as the cellular problems P^j_{cell}, for $1 \leqslant j \leqslant k$, are supposed to be solved, so that $\underset{\sim}{\acute{\mathbf{e}}}^{k-1}$ and $\partial_3\underset{\sim}{\acute{\mathbf{e}}}^{k-2}$ and the matrices $\boldsymbol{\chi}^1$, $\boldsymbol{\chi}^2$ and $\boldsymbol{\tau}^1$, $\boldsymbol{\tau}^2$ are known. Consequently, Eqs. (42) and (43) enable us the derivation of three boundary conditions for the P^k_{hom} problem, which complete the kth order equations for the macroscopic stresses given in Eq. (30).

Case (C): This is the complement of Case B. First, relation (23) provides the boundary conditions for the successive axial forces $N^k(z_3)$ and bending moments $M^k_\alpha(z_3)$:

$$\begin{aligned} &N^1(0) = \int_{S_0}\bar{\sigma}_{33}\,\mathrm{d}y_1\,\mathrm{d}y_2, \qquad M^1_\alpha(0) = \int_{S_0} -y_\alpha\bar{\sigma}_{33}\,\mathrm{d}y_1\,\mathrm{d}y_2 \\ &N^k(0) = M^k_\alpha(0) = 0 \quad \text{for } k \geqslant 2 \end{aligned} \tag{44}$$

At each order $k \geqslant 1$, the macroscopic boundary conditions are constituted of one of the preceding sets of three equations and three others involving the macroscopic deflections $\hat{u}_\alpha^{k-1}$ and the twisting angle φ^k. These conditions are derived from Eq. (24), following a similar procedure as in Case B, but with the state (2) corresponding to the Saint-Venant unit flexure solutions (VF_β) and torsion solutions (VT) respectively. The details of the calculations are omitted here and the so derived coupled boundary conditions are given below.

$$P^1_{\mathrm{hom}}\begin{cases} \hat{u}^0_\beta(0) = \int_{S_0}\bar{u}_\alpha\sigma_{\alpha 3}^{(\mathrm{VF}_\beta)}\,\mathrm{d}y_1\,\mathrm{d}y_2 \\ \varphi^1(0) - \left(\int_{S_0}\tau^1_{33\mathbf{m}}u_3^{(\mathrm{VT})}\,\mathrm{d}y_1\,\mathrm{d}y_2\right)\acute{e}^1_{\mathbf{m}}(0) = -\int_{S_0}\bar{\sigma}_{33}u_3^{(\mathrm{VT})}\,\mathrm{d}y_1\,\mathrm{d}y_2 \end{cases} \tag{45}$$

$$P^2_{\mathrm{hom}}\begin{cases} \hat{u}^1_\beta(0) = \int_{S_0}(\tau^1_{33\mathbf{m}}\acute{e}^1_{\mathbf{m}}(0) - \bar{\sigma}_{33})u_3^{(\mathrm{VF}_\beta)}\,\mathrm{d}y_1\,\mathrm{d}y_2 \\ \varphi^2(0) - \left(\int_{S_0}\tau^1_{33\mathbf{m}}u_3^{(\mathrm{VT})}\,\mathrm{d}y_1\,\mathrm{d}y_2\right)\acute{e}^2_{\mathbf{m}}(0) = \int_{S_0}\left(\tau^2_{33\mathbf{m}}\partial_3\acute{e}^1_{\mathbf{m}}(0)u_3^{(\mathrm{VT})} - \chi^1_{\alpha\mathbf{m}}\acute{e}^1_{\mathbf{m}}(0)\sigma_{\alpha 3}^{(\mathrm{VT})}\right)\mathrm{d}y_1\,\mathrm{d}y_2 \end{cases} \tag{46}$$

$$P^k_{\mathrm{hom}}, k \geqslant 3\begin{cases} \hat{u}^{k-1}_\beta(0) = \int_{S_0}\Big[(\tau^1_{33\mathbf{m}}\acute{e}^{k-1}_{\mathbf{m}}(0) + \tau^2_{33\mathbf{m}}\partial_3\acute{e}^{k-2}_{\mathbf{m}}(0))u_3^{(\mathrm{VF}_\beta)} - (\chi^1_{\alpha\mathbf{m}}\acute{e}^{k-2}_{\mathbf{m}}(0) \\ \qquad + \chi^2_{\alpha\mathbf{m}}\partial_3\acute{e}^{k-3}_{\mathbf{m}}(0))\sigma_{\alpha 3}^{(\mathrm{VF}_\beta)}\Big]\,\mathrm{d}y_1\,\mathrm{d}y_2 \\ \varphi^k(0) - \left(\int_{S_0}\tau^1_{33\mathbf{m}}u_3^{(\mathrm{VT})}\,\mathrm{d}y_1\,\mathrm{d}y_2\right)\acute{e}^k_{\mathbf{m}}(0) \\ \quad = \int_{S_0}\Big[(\tau^2_{33\mathbf{m}}\partial_3\acute{e}^{k-1}_{\mathbf{m}}(0))u_3^{(\mathrm{VT})} - (\chi^1_{\alpha\mathbf{m}}\acute{e}^{k-1}_{\mathbf{m}}(0) + \chi^2_{\alpha\mathbf{m}}\partial_3\acute{e}^{k-2}_{\mathbf{m}}(0))\sigma_{\alpha 3}^{(\mathrm{VT})}\Big]\,\mathrm{d}y_1\,\mathrm{d}y_2 \end{cases} \tag{47}$$

Case (D): The boundary conditions for this case are derived from Eq. (25). At a given order k, they lead to classical displacement data, corresponding to prescribed values for $\{\hat{u}_3^k(0), \hat{u}_\alpha^{k-1}(0), \varphi^k(0)\}$, i.e. the unknowns of the P^k_{hom} problem. These edge data present the feature of involving the six fundamental cantilever beam solutions and are given below:

$$P^1_{\text{hom}}\begin{cases}\hat{u}^0_\beta(0)=\int_{S_0}\bar{u}_\alpha\sigma^{(\text{BF}_\beta)}_{\alpha 3}\,\text{d}y_1\,\text{d}y_2\\ \hat{u}^1_3(0)=\int_{S_0}\bar{u}_3\sigma^{(\text{BE})}_{33}\,\text{d}y_1\,\text{d}y_2\\ \partial_3\hat{u}^0_\beta(0)=\int_{S_0}\bar{u}_3\sigma^{(\text{BB}_\beta)}_{33}\,\text{d}y_1\,\text{d}y_2\\ \varphi^1(0)=\int_{S_0}\bar{u}_3\sigma^{(\text{BT})}_{33}\,\text{d}y_1\,\text{d}y_2\end{cases}\tag{48}$$

$$P^2_{\text{hom}}\begin{cases}\hat{u}^1_\beta(0)=0\\ \hat{u}^2_3(0)=-(\int_{S_0}\chi^1_{i\mathbf{m}}\sigma^{(\text{BE})}_{i3}\,\text{d}y_1\,\text{d}y_2)\cdot\acute{e}^1_{\mathbf{m}}(0)\\ \partial_3\hat{u}^1_\beta(0)=-(\int_{S_0}\chi^1_{i\mathbf{m}}\sigma^{(\text{BB}_\beta)}_{i3}\,\text{d}y_1\,\text{d}y_2)\cdot\acute{e}^1_{\mathbf{m}}(0)\\ \varphi^2(0)=-(\int_{S_0}\chi^1_{i\mathbf{m}}\sigma^{(\text{BT})}_{i3}\,\text{d}y_1\,\text{d}y_2)\cdot\acute{e}^1_{\mathbf{m}}(0)\end{cases}\tag{49}$$

$$P^k_{\text{hom}},k\geqslant 3\begin{cases}\hat{u}^{k-1}_\beta(0)=-\int_{S_0}(\chi^1_{j\mathbf{m}}\cdot\acute{e}^{k-2}_{\mathbf{m}}(0)+\chi^2_{j\mathbf{m}}\cdot\partial_3\acute{e}^{k-3}_{\mathbf{m}}(0))\sigma^{(\text{BF}_\beta)}_{j3}\,\text{d}y_1\,\text{d}y_2\\ \hat{u}^k_3(0)=-\int_{S_0}(\chi^1_{j\mathbf{m}}\cdot\acute{e}^{k-1}_{\mathbf{m}}(0)+\chi^2_{j\mathbf{m}}\cdot\partial_3\acute{e}^{k-2}_{\mathbf{m}}(0))\sigma^{(\text{BE})}_{j3}\,\text{d}y_1\,\text{d}y_2\\ \partial_3\hat{u}^{k-1}_\beta(0)=-\int_{S_0}(\chi^1_{j\mathbf{m}}\cdot\acute{e}^{k-1}_{\mathbf{m}}(0)+\chi^2_{j\mathbf{m}}\cdot\partial_3\acute{e}^{k-2}_{\mathbf{m}}(0))\sigma^{(\text{BB}_\beta)}_{j3}\,\text{d}y_1\,\text{d}y_2\\ \varphi^k(0)=-\int_{S_0}(\chi^1_{j\mathbf{m}}\cdot\acute{e}^{k-1}_{\mathbf{m}}(0)+\chi^2_{j\mathbf{m}}\cdot\partial_3\acute{e}^{k-2}_{\mathbf{m}}(0))\sigma^{(\text{BT})}_{j3}\,\text{d}y_1\,\text{d}y_2\end{cases}\tag{50}$$

Different examples will now be treated in order to illustrate the method.

4. Numerical examples

4.1. Presentation of the treated examples

The periodic structure considered for the examples is a lattice with rigid joints (Virendeel girder) shown in Fig. 1. Each member of the lattice is a beam of square cross-section 1×1 mm^2, and $l=40$ mm, $h=39$ mm, with h the distance between the centroids of the horizontal beams, so that the overall height of the lattice is 40 mm. The constitutive material is isotropic with a Poisson ratio $\nu=0.3$. Concerning the Young modulus, two cases will be considered, see Fig. 1: in the first case, corresponding to the symmetric case, $E=200\,000$ MPa for all the beams of the lattice. In the second case (asymmetric case), in order to introduce a coupling between the stretching and the bending of the structure, the horizontal beams of the upper face of the lattice have $E=400\,000$ MPa, while $E=200\,000$ MPa in the rest of the lattice.

Two different boundary value problems will be considered. The first one is the cantilever beam with an end transverse shearing force in the $\mathbf{e_1}$-direction, see Fig. 2(a), so that the boundary conditions D and A hold at the ends S^ε_0 and S^ε_L respectively, i.e.:

Case (D) displacement data at S^ε_0

$$u^\varepsilon_i(x_1,x_2,0)=0\tag{51}$$

Case (A) stress data at S^ε_L

$$\begin{cases}\sigma^\varepsilon_{13}(x_1,x_2,0)=\bar{\sigma}^\varepsilon_{13}\\ \sigma^\varepsilon_{23}(x_1,x_2,0)=\sigma^\varepsilon_{33}(x_1,x_2,0)=0\end{cases}\tag{52}$$

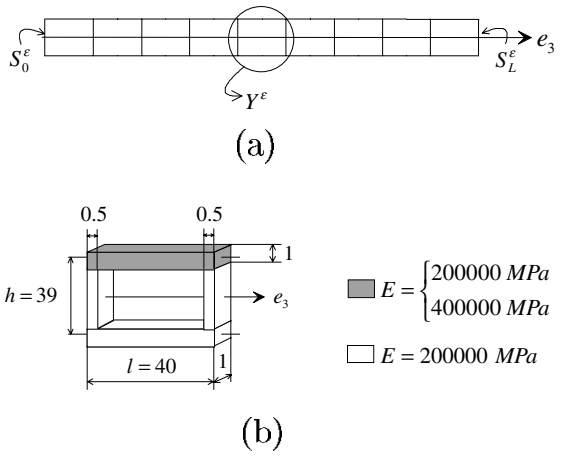

Fig. 1. (a) The Virendeel girder; (b) the periodicity cell.

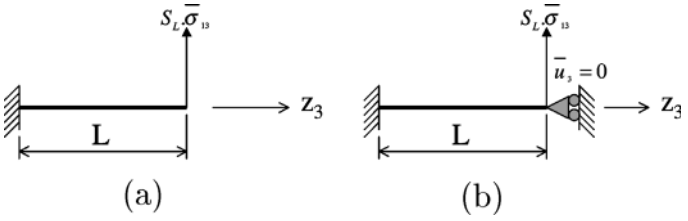

Fig. 2. The boundary value problems: (a) boundary conditions D–A; (b) boundary conditions D–B.

The second example is slightly different, see Fig. 2(b): the beam is still clamped at the end S_0^ε, but instead of the prescribed data (52) at S_L^ε, the following mixed boundary conditions B are considered:

Case (B) mixed data at S_L^ε

$$\begin{cases} \sigma_{13}^\varepsilon(x_1, x_2, 0) = \bar{\sigma}_{13}^\varepsilon \\ \sigma_{23}^\varepsilon(x_1, x_2, 0) = 0 \\ u_3^\varepsilon(x_1, x_2, 0) = \bar{u}_3^\varepsilon = 0 \end{cases} \tag{53}$$

These two problems are symmetric with respect to the $\underset{\sim}{\mathbf{e}_1}$–$\underset{\sim}{\mathbf{e}_3}$ plane, and consequently, in the following, we will restrict the study in that plane.

In the next section, numerical results will be presented for the symmetric lattice considering both boundary value problems, and for the asymmetric lattice in the case of the first boundary value problem.

4.2. Results – comparison between the asymptotic solution and the exact one

On the one hand, the outer asymptotic solution is derived, following the method described previously. First, the first two microscopic cellular problems P^0_{cell} and P^1_{cell} with the periodicity cell shown in Fig. 1 have been solved via the finite element method, in the symmetric and asymmetric cases. Thus, for each case, the

periodic fields $\boldsymbol{\chi}^1(\mathbf{y})$, $\boldsymbol{\chi}^2(\mathbf{y})$, $\boldsymbol{\tau}^1(\mathbf{y})$, $\boldsymbol{\tau}^2(\mathbf{y})$ of the expansions (7) and (8), and consequently the effective stiffness matrices $\mathscr{A}^{\text{hom1}}$, $\widetilde{\mathscr{A}}^{\text{hom2}}$ are determined, with the reference axis of the beam taken as its centroidal axis. Thus, in the symmetric case, the matrix associated with $\mathscr{A}^{\text{hom1}}$ is found to be diagonal, while in the asymmetric case, there is an extra-diagonal term for the coupling between the stretching and the bending in the $\underset{\sim}{\mathbf{e_1}}$–$\underset{\sim}{\mathbf{e_3}}$ plane.

Then, at each order and following the method described in Section 3, the boundary conditions for the 1D macroscopic problems are derived. To this end, Saint-Venant's solutions and the fundamental cantilever beam solutions are computed from a finite element model with several periods. The determination of these boundary conditions enable us to solve the successive 1D P^i_{hom} problems. Analytical and semi-analytical solutions are obtained for the first and second boundary value problems respectively, see Buannic (2000). In that way, the asymptotic expansion of the macroscopic description of the displacements of the structure is derived, corresponding in 2D to:

$$\begin{aligned} \hat{u}_1(z_3) &= \hat{u}_1^0(z_3) + \varepsilon\hat{u}_1^1(z_3) + \cdots \\ \hat{u}_3(z_3) &= \varepsilon\hat{u}_3^1(z_3) + \varepsilon^2\hat{u}_3^2(z_3) + \cdots \end{aligned} \tag{54}$$

where $\hat{u}_1(z_3)$ and $\hat{u}_3(z_3)$ denote the macroscopic deflection and macroscopic axial displacement respectively.

On the other hand, the reference 3D heterogeneous solutions are computed from a detailed finite element model of the corresponding boundary value problem. The comparison between these reference solutions and the asymptotic ones are given in the next subsections, enabling us to analyze the accuracy of the asymptotic method including correction due to edge effects.

4.2.1. First boundary value problem: boundary conditions D–A

For this problem and as shown in Buannic (2000), the asymptotic expansions stop at the third order, which means that summing the successive solutions up to the third order give the whole expansion, so that Eq. (54) is simply restricted to:

$$\begin{aligned} \hat{u}_1(z_3) &= \hat{u}_1^0(z_3) + \varepsilon\hat{u}_1^1(z_3) + \varepsilon^2\hat{u}_1^2(z_3) + \varepsilon^3\hat{u}_1^3(z_3) \\ \hat{u}_3(z_3) &= \varepsilon\hat{u}_3^1(z_3) + \varepsilon^2\hat{u}_3^2(z_3) + \varepsilon^3\hat{u}_3^3(z_3) \end{aligned} \tag{55}$$

Results for the symmetric and asymmetric cases are shown in Fig. 3. Fig. 3(a) and (b) shows the deflection $\hat{u}_1(z_3)$ in the symmetric case, for a structure constituted with 10 and 20 periods respectively. Fig. 3(c) and (d) represent the deflection in the asymmetric case, and Fig. 3(e) and (f) the axial displacement $\hat{u}_3(z_3)$ in that case, since the stretching/bending coupling leads then to produce a non-zero axial displacement.

On these figures, the *first order solution* denotes the asymptotic expansion (55) summed up to the first order term with respect to ε, the *second order solution* the expansion up to the second order term, and the *third order solution* stands thus for the whole expansion (55). The 3D heterogeneous solution is computed with a detailed finite element model of the structure with brick elements, which is obtained from the repetition of the mesh of the period used for the cellular problems. The overall deflection and axial displacement drawn on the figures correspond to the displacements of the middle axis $x_\alpha = 0$ of the heterogeneous structure.

Remark 4.1. The solution of the cellular problems is defined up to a rigid body displacement composed of the three translations and the rotation about the $\mathbf{e_3}$-axis (see Section 4.1 in Part I). Thus, in the finite element analysis of these problems, three degrees of freedom of one node and one degree of freedom of another node have to be set to zero. In the present examples, the following conditions have been prescribed:

$$\underset{\sim}{\boldsymbol{\chi}}^1(y_\alpha = 0, y_3^-) = \underset{\sim}{\boldsymbol{\chi}}^1(y_\alpha = 0, y_3^+) = \underset{\sim}{\boldsymbol{\chi}}^2(y_\alpha = 0, y_3^-) = \underset{\sim}{\boldsymbol{\chi}}^2(y_\alpha = 0, y_3^+) = \underset{\sim}{\mathbf{0}},$$

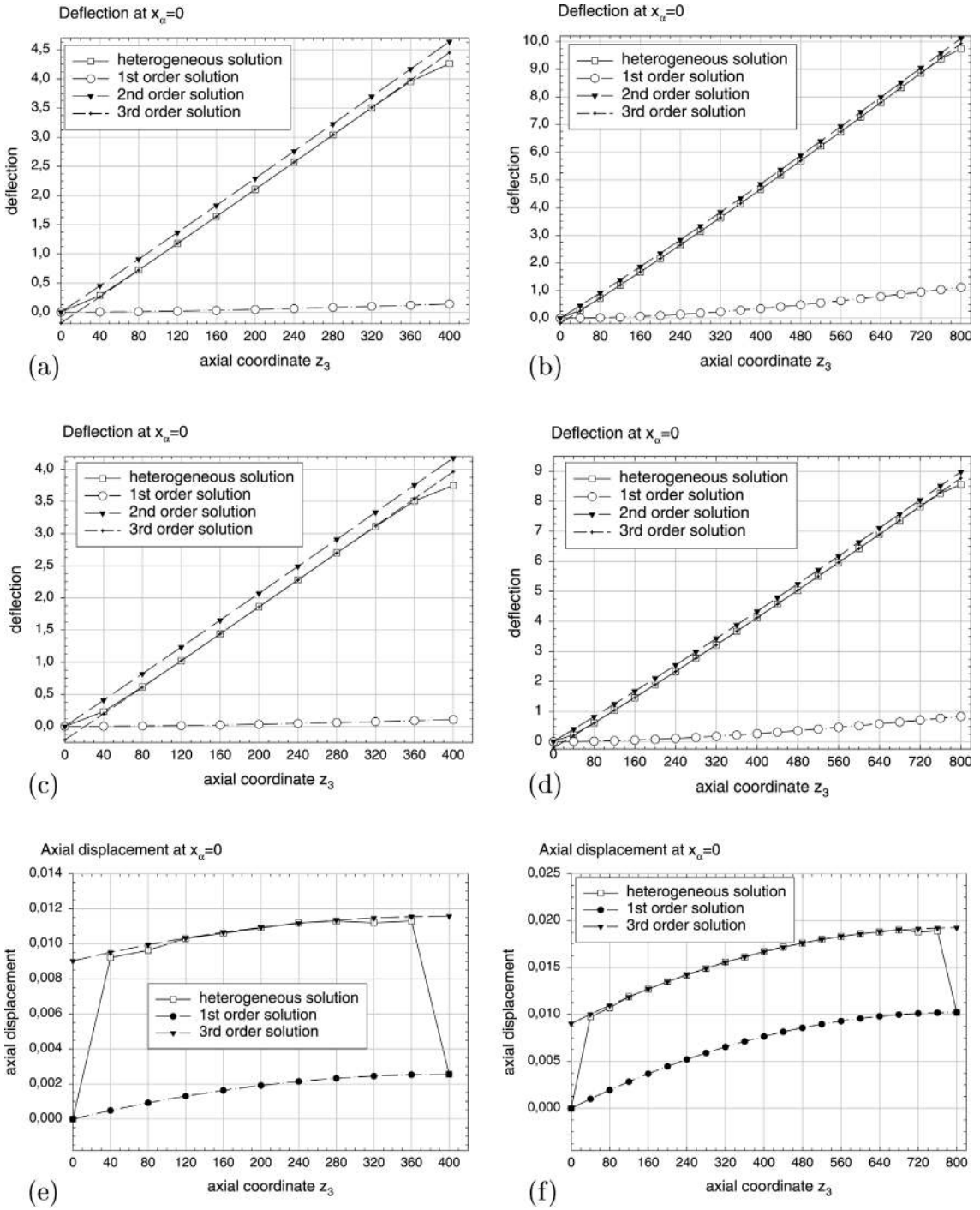

Fig. 3. Results for the cantilever beams. Deflection of the symmetric lattice: (a) 10 periods; (b) 20 periods. Deflection of the asymmetric lattice: (c) 10 periods; (d) 20 periods. Axial displacement of the asymmetric lattice: (e) 10 periods; (f) 20 periods.

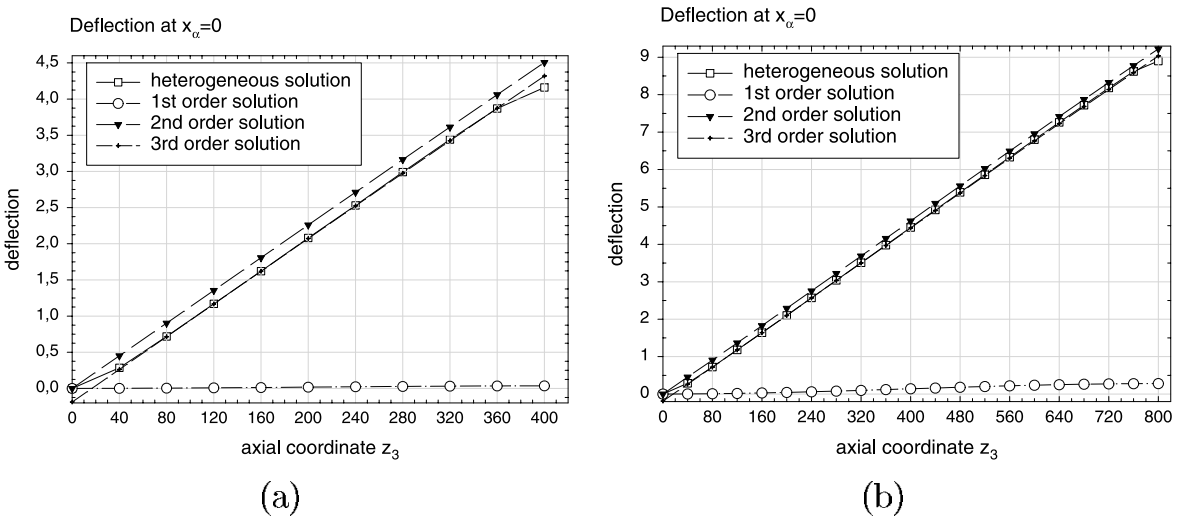

Fig. 4. Deflection of the symmetric beam – prescribed data D and B: (a) 10 periods; (b) 20 periods.

where y_3^- and y_3^+ correspond to the y_3-coordinate of the end sections of the period ∂Y_a^- and ∂Y_a^+ respectively. So, from Eq. (7), when z_3 is equal to a whole number of periods, the outer expansion $\underset{\sim}{\mathbf{u}}^{(I)}$ is equal to the macroscopic solution given in Eq. (54).

It can be seen from all the figures that the first order solution gives a very bad estimation of the exact solution (it becomes satisfactory for a number of periods reaching 50) and emphasizes that the beam studied here is very weak in shear. A significant improvement is given by the second order solution, and the agreement between the solution computed up to the third order (i.e. the whole expansion) and the 3D heterogeneous solution is very good. The only difference results from edge effects, the length of which is about one period for the symmetric case, between one and two periods for the deflection in the asymmetric case, and between two and three periods for the axial displacement in the asymmetric case.

4.2.2. Second boundary value problem: boundary conditions D–B

In that case, results similar to those of the cantilever beam are found, see Fig. 4. The only difference concerns the second order macroscopic deflection $\hat{u}_1^2$, which is quadratic with respect to z_3.

5. Concluding remarks

In this paper, the decay analysis technique proposed in Gregory and Wan (1984) has been used for a heterogeneous beam. Thus, the appropriate set of boundary conditions for the successive terms of the interior expansion has been derived, considering arbitrary 3D stress, displacement or mixed edge data. These boundary conditions are such that the difference between the full asymptotic outer solution and the exact 3D one remains significant only near the edges. In the case of stress data, this method enables us to justify rigorously the application of Saint-Venant's principle. For displacement or mixed data, the method leads to unconventional boundary conditions, which may introduce possible couplings, even if the latter do not appear in the homogenized constitutive law.

The main interest of the decay analysis technique is to incorporate the edge effects in the asymptotic beam model, without computing any inner expansion, in contrast to the matching method. In particular, if

the beam is loaded only on its end sections, the boundary conditions for the outer expansion are obtained from the numerical solution of only two cellular problems and a set of 3D canonical beam problems.

In Section 4 of this paper, different examples on a lattice structure with a possible stretching-bending coupling, are treated. It is shown that the method leads to the approximation of the exact 3D outer solution with a very good accuracy. Other applications of this asymptotic method including corrections due to end effects can be found in Buannic and Cartraud (2000) where the case of heterogeneous composite beams is considered.

Lastly, it has been illustrated here that the inclusion of higher-order terms of the interior expansion in a beam theory will actually improve the approximation of the 3D solution provided that edge effects are taken into account (similar conclusions hold in the case of plates, see Goldenveizer et al. (1993)). In that sense, other authors claimed that considering end effects makes the use of a refined beam or plate theory unnecessary (Duva and Simmonds, 1991; Gregory and Wan, 1984). Our results agree with such a conclusion, since the full outer displacement is found to be the solution of the classical Euler–Bernoulli differential equations, if the beam is loaded only on its end sections. Consequently, in that case, the present asymptotic beam model differs from the classical engineering one only through the expression of the boundary conditions, which have to incorporate corrections due to edge effects.

Acknowledgements

The authors gratefully acknowledge Professor J.G. Simmonds (University of Virginia) for fruitful discussions, useful advices, and encouragements during the preparation of this work. The authors also wish to express their appreciation to Dr. S. Bourgeois (LMA Marseille, France), for helpful ideas and comments.

References

Buannic, N., 2000. Analyse asymptotique de poutres élastiques hétérogènes. Ph.D. Thesis, Ecole Centrale de Nantes, France.

Buannic, N., Cartraud, P., 2000. Higher-order asymptotic beam model including corrections due to end effects. Proceedings of the 41st AIAA/ASME/ASCE/AHS/ASC Structures, Structural Dynamics and Materials Conference, Atlanta, Georgia. AIAA Paper 2000-1495.

Dauge, M., Gruais, I., Rőssle, A., 1999. The influence of lateral boundary conditions on the asymptotics in thin elastic plates. SIAM Journal on Mathematical Analysis 31, 305–345.

Dumontet, H., 1990. Homogénéisation et effets de bords dans les matériaux composites. Thesis, Université Paris 6.

Duva, J.M., Simmonds, J.G., 1991. The usefulness of elementary theory for the linear vibrations of layered, orthotropic elastic beams and corrections due to two-dimensional end effects. Journal of Applied Mechanics 58, 175–180.

Fan, H., 1989. On the foundations of beam theory. Ph.D. Thesis, University of Illinois, Chicago.

Fan, H., Widera, G.E.O., 1992. On the proper boundary conditions for a beam. Journal of Applied Mechanics 59, 915–922.

Friedrichs, K., Dressler, R., 1961. A boundary layer theory for elastic plates. Communications on Pure and Applied Mathematics XIV, 1–33.

Goldenveizer, A.L., Kaplunov, J.D., Nolde, E.V., 1993. On Timoshenko–Reissner type theories of plates and shells. International Journal of Solids and Structures 30 (5), 675–694.

Gregory, R.D., Gladwell, I., 1982. The cantilever beam under tension, bending or flexure at infinity. Journal of Elasticity 12, 317–343.

Gregory, R.D., Wan, Y.M.F., 1984. Decaying states of plane strain in a semi-infinite strip and boundary conditions for plate theory. Journal of Elasticity 14, 27–64.

Horgan, C.O., 1989. Recent developments concerning Saint-Venant's principle: An update. Applied Mechanics Reviews 42 (11), 295–303.

Horgan, C.O., 1996. Recent developments concerning Saint-Venant's principle: A second update. Applied Mechanics Reviews Part 2 49 (10), 101–111.

Irago, H., 1999. A Saint-Venant's analysis in free elastic rods. Comptes Rendus de l'Académie des Sciences, Série I 329 (6), 557–562.

Irago, H., Viaño, J.M., 1999. Error estimation in the Bernoulli–Navier model for elastic rods. Asymptotic Analysis 21 (1), 71–87.

Kolpakov, A.G., 1991. Calculation of the characteristics of thin elastic rods with a periodic structure. Journal of Applied Mathematics and Mechanics 55 (3), 358–365.
Rigolot, A., 1976. Sur une théorie asymptotique des poutres droites. Thesis, Université Paris 6.
Stephen, N.G., Wang, P.J., 1996. On Saint-Venant's principle in pin-jointed frameworks. International Journal of Solids and Structures 33 (1), 79–97.
Timoshenko, S.P., Goodier, J.N., 1970. Theory of Elasticity, third edn., McGraw-Hill, New York.